Int. J. Heat Mass Transfer. Vol. 36, No. 15, pp. 3731–3741, 1993
Printed in Great Britain

0017–9310/93 $6.00+0.00

Non-ideal vaporization of dilating binary droplets with variable properties

P. L. C. LAGE,† C. M. HACKENBERG‡ and R. H. RANGEL†

† Department of Mechanical and Aerospace Engineering, University of California at Irvine, Irvine, CA 92717, U.S.A.

‡ Programa de Engenharia Química, COPPE, Universidade Federal do Rio de Janeiro, Caixa Postal 68502, 21945 Rio de Janeiro, Brazil

(*Received* 29 *October* 1992 *and in final form* 5 *March* 1993)

Abstract—A diffusive liquid vaporization model for multicomponent droplets has been developed. It includes: spatially and time dependent density, the interdiffusion term in the energy equation, variable properties, and non-ideal phase equilibrium. This model is used to simulate the vaporization of monocomponent droplets of *n*-heptane and methanol, and bicomponent droplets of their mixture. It is shown that density variations induce an internal convection which, together with the interdiffusion of species, results in a significant decrease of the droplet lifetime and the energy requirement for vaporization when compared with the predictions of the more traditional model. It is also found that the surface conditions are primarily controlled by phase equilibrium. The model is able to predict the experimentally-observed sparkle at the end of droplet combustion.

INTRODUCTION

As NATURAL fossil-fuel resources begin to show their inability to support mankind's development indefinitely, alternative energy sources and fuels have received much attention in the past years. Combustion scientists have examined the use of synthetic fuel blends with high boiling point liquids or coal, thus increasing the availability of lighter fuels for petrochemical use. Another trend is the use of renewable fuels in blends (ethanol in gasoline and diesel). The vaporization of the heavier fuels is important, and sometimes a controlling factor, in the determination of the combustion efficiency, while the non-ideal behavior of alcohol–hydrocarbon mixtures is too pronounced to be neglected. Therefore, a great deal of research has been carried out in the past years to increase our fundamental understanding of vaporization and combustion of multicomponent liquid droplets [1, 2]. Some aspects of the droplet vaporization theory have been experimentally confirmed, although the agreement is sometimes only qualitative. Furthermore, there are some experimental facts on droplet micro-explosion that need a theoretical explanation [3]. Thus, theoretical research on the specific characteristics of multicomponent droplet vaporization is essential to bring theory and experiment to an agreement.

The theory of monocomponent droplet vaporization evolved from the pure gas-phase model ('d^2-law' with constant liquid temperature) to the liquid-phase uniform temperature model (infinite-conductivity model [4]) and then to the liquid-phase convective–diffusive models [5, 6]. This evolution reflects the increasing importance of the heating and vaporization of heavy fuels in the overall process. It is now well understood that liquid heat diffusion is the controlling mechanism for both the stagnant droplet vaporization (diffusion-limit model [5]) and the droplet vaporization in a convective field (convective models [6, 7]), as supported by experimental evidence [8]. In the latter case the diffusion is basically normal to the streamlines of internal circulation. For multicomponent fuels, mass diffusion is much slower than heat diffusion and it is then the controlling factor. Extensions for the diffusive and convective models have been developed [9, 10]. However, none of the above models incorporate the interdiffusion term in the energy equation or the allowance for transient density field due to temperature and concentration changes. Interdiffusion and variable density have been considered in fully numerical computations for a convective flow that include the velocity, temperature and concentration fields [11], but the importance of these effects is not analyzed. The inclusion of bulk change of density has already been incorporated in the conventional diffusive model [8], but no radial dependence was allowed. Moreover, all the above models assume that there exists phase equilibrium at the droplet surface, using the simple integrated form of the Clausius–Clapeyron equation and ideal solution behavior to calculate the vapor concentrations at the surface. A better saturated-pressure dependence has been used by Lage and Rangel [12] in a study of radiation absorption in monocomponent droplet vaporization. Although there is a considerable interest in non-ideal fuel mixtures, vaporization models so far have ignored the non-ideal phase equilibrium.

The explosive vaporization of multicomponent mixtures has been predicted theoretically [9] and con-

NOMENCLATURE

a	activity coefficient
b	coefficient in Wilson's equation
c_p	specific heat at constant pressure
D	binary diffusion coefficient
f_m	fraction of the initial droplet mass
h	specific enthalpy, $\int_{T_o}^{T} c_p \, dT = c_{p_m}(T-T_o)$
k	thermal conductivity
L	latent heat of vaporization
$\dot{m}$	mass rate of vaporization
P	pressure
Q_G	rate of heat transfer from the gas phase
Q_R	volumetric radiant heat absorption
r	radial coordinate
R	droplet radius
R_g	gas constant
t	time
T	temperature
v	radial velocity
V	dimensionless velocity, $R_o v/\alpha_o$
$\mathscr{V}$	molar volume
x	liquid molar fraction
Y	mass fraction
y	gas molar fraction.

Greek symbols

α	thermal diffusivity
β	dimensionless droplet radius, $R(t)/R_o$
ε	fractional mass vaporization rate, $\dot{m}_i/\dot{m}$
η	dimensionless radial coordinate, $r/R(t)$
Θ	dimensionless temperature, $(T-T_o)/(T_r-T_o)$
ρ	density
τ	dimensionless time, $\alpha t/R_o^2$
ϕ	fugacity coefficient.

Subscripts

i, j	substance
m	mean
o	initial
r	reference
s	surface.

Superscripts

L	liquid phase
sat	saturation
$\bar{}$	partial quantity
$\hat{}$	mixture.

firmed experimentally [3, 8, 13] for a low Reynolds number droplet. The agreement of theory and experiment is fairly good. The predicted trends of necessary volatility differentials and influence of concentration and pressure have been verified by experiments [3, 8, 13]. However, the radial positions at which bubbles are formed are much closer to the droplet center than the conventional diffusive model predicts [8], which corresponds to a larger heat diffusion in the droplet than the model prediction. Such an effect can be caused by the neglect of the interdiffusion term in the energy conservation equation and/or the constant density assumption. Another interesting observation is the fact that alcohol–alkane mixtures undergo explosive vaporization only if the alcohol is the more volatile component [3]. It was pointed out that the non-ideality of the liquid mixture *could* lead to a lower nucleation temperature (alcohols with low molecular weight form highly non-ideal solutions with alkanes, while heavier alcohols form more ideal mixtures with alkanes). Although it is necessary to study the nucleation of non-ideal mixtures, non-ideal phase equilibrium must be incorporated into the vaporization models to verify its effects on the transient droplet temperature and concentration fields. Another interesting experimental fact is that, when no disruptive burning occurs, the combustion of pure-substance or mixture droplets ends with a weak sparkle that is assumed to be caused by the microexplosion of the very small droplets due to the presence of heavy impurities in the fuels [3, 8].

From the above argument, it is clear that some aspects of the droplet vaporization modeling need further investigation. In this work, we develop a liquid-phase diffusive model for a multicomponent droplet with variable properties including the interdiffusion term in the energy equation, the variable density field caused by temperature and concentration changes, and non-ideal phase equilibrium at the droplet surface. Our aim is to quantify the specific effects of these processes and to possibly explain some experimental results.

GOVERNING EQUATIONS

Under the assumptions of negligible internal circulation and spherical symmetry, the mass, species, and energy conservation equations for a binary spherical droplet can be written as

$$\frac{\partial \rho}{\partial t} + \frac{1}{r^2}\frac{\partial}{\partial r}(r^2 \rho v) = 0 \tag{1}$$

$$\frac{\partial Y_i}{\partial t} + v\frac{\partial Y_i}{\partial r} = \frac{1}{r^2 \rho}\frac{\partial}{\partial r}\left(r^2 \rho D \frac{\partial Y_i}{\partial r}\right), \quad i = 1,2 \tag{2}$$

$$\frac{\partial T}{\partial t} + v\frac{\partial T}{\partial r} = \frac{1}{r^2 \rho c_p}\left[\frac{\partial}{\partial r}\left(r^2 k \frac{\partial T}{\partial r}\right) - (\bar{h}_1 - \bar{h}_2)\frac{\partial}{\partial r}\left(r^2 \rho D \frac{\partial Y_1}{\partial r}\right) + Q_R\right] \tag{3}$$

with the following boundary conditions obtained by

mass, species and energy balances at the droplet surface

$$r = R(t), \quad -4\pi R^2 \rho D \frac{\partial Y_i}{\partial r} + \dot{m} Y_i = \dot{m}\varepsilon_i, \quad i = 1,2 \tag{4}$$

$$r = R(t), \quad -k\frac{\partial T}{\partial r} + \rho v \sum_{i=1}^{2} \bar{h}_i Y_i - \rho D \sum_{i=1}^{2} \bar{h}_i \frac{\partial Y_i}{\partial r} + \rho \frac{\mathrm{d}R}{\mathrm{d}t} \sum_{i=1}^{2} \varepsilon_i \bar{L}_i = -\frac{Q_G}{4\pi R^2} \tag{5}$$

where the radial surface velocity is given by

$$v_s = \frac{\dot{m}}{4\pi R^2 \rho_s} + \frac{\mathrm{d}R}{\mathrm{d}t}. \tag{6}$$

No heat absorption by radiation is considered in this analysis ($Q_R = 0$). Note that equations (1) and (2) are not all linearly independent, and one of the species conservation equations does not need to be considered. It should also be noted that v represents the internal radial velocity without circulation which is entirely due to density changes. We can integrate the continuity equation (equation (1)) with the boundary condition ($r = 0$, v finite) to obtain the velocity profile inside the droplet

$$v(r,t) = -\frac{1}{r^2\rho}\int_0^r r'^2 \frac{\partial \rho}{\partial t}\,\mathrm{d}r' \tag{7}$$

and $v(0,t) = 0$ by the limit process, as expected from physical reasoning.

By definition, the mass vaporization rate can be obtained by differentiating the integrated droplet mass. Using Leibnitz rule for integrals, the radius rate of change can be expressed by

$$\frac{\mathrm{d}R}{\mathrm{d}t} = -\frac{\dot{m}}{4\pi\rho_s R^2} - \frac{1}{\rho_s R^2}\int_0^R r^2 \frac{\partial \rho}{\partial t}\,\mathrm{d}r \tag{8}$$

which, using equation (7) at $r = R$, is identical to equation (6).

The above formulation is restricted to binary systems because of the Fickian form used for the mass diffusion term in equation (2) (which is exact for binary mixtures and only an approximation for multicomponent systems) and the simplified form of the interdiffusion term which appears in equation (3) (where $\mathrm{d}Y_1 = -\mathrm{d}Y_2$ has been used). Thus, with minor modifications, the above equations are valid for multicomponent droplet vaporization.

In this liquid-phase model, $\dot{m}$, ε_i and Q_G are parameters given by a coupled gas-phase model and represent the mass and energy transfer between the two phases. In this work, we use the extended film theory for the gas-phase model developed by Abramzon and Sirignano [7], together with the heat and mass transfer correlations obtained by Lage *et al.* [14] to extend the analysis to multicomponent mixtures. This procedure matches the results from the film theory [15] with the boundary-layer results [14], providing a convective correction factor for the mass vaporization given by the former. Although we will focus the analysis on stagnant droplets, because the hypothesis of negligible circulation is then warranted, the continuous and dispersed-phase models are not limited to such cases.

Non-ideal phase equilibrium

Phase equilibrium is assumed at the droplet surface. The gas is still assumed to be ideal but the liquid phase activity coefficients are calculated by Wilson's equation based on experimental data (at 1 atm and basically at 333 K for the *n*-heptane–methanol mixture [16]). The Wilson equation parameters are extrapolated to higher temperatures using their approximated temperature dependence and correlations for the liquid densities [17]. The equilibrium equations can be summarized by

$$a_i x_i P_i^{\mathrm{sat}} \phi_i^{\mathrm{sat}} \mathscr{P} = y_i P \hat{\phi}_i, \quad i = 1,2 \tag{9}$$

$$\mathscr{P} = \exp\left[\int_{P_i^{\mathrm{sat}}}^{P} \frac{\mathscr{V}_i^{\mathrm{L}}}{R_g T}\,\mathrm{d}P\right] \tag{10}$$

$$\ln a_i = -\ln(x_i + b_{ij}x_j) + x_j\left(\frac{b_{ij}}{x_i + b_{ij}x_j} - \frac{b_{ji}}{b_{ji}x_i + x_j}\right), \quad i = 1,\ j = 2 \quad \text{or} \quad i = 2,\ j = 1 \tag{11}$$

where

$$b_{ij} = \frac{\mathscr{V}_j^{\mathrm{L}}}{\mathscr{V}_i^{\mathrm{L}}}\exp\left(-\frac{C_{ij}}{R_g T}\right) \tag{12}$$

and the saturation pressure of each substance is calculated by Wagner's equation [17]. The liquid molar volumes are assumed equal to the saturated volumes (and thus pressure-independent) and calculated by the modified Rackett equation [17] based on known data [18]. The ideal-gas assumption for the gas phase was made due to lack of binary interaction parameters between air (or nitrogen and oxygen) and the liquid components for the Peng–Robinson equation [19] used to calculate gas fugacities. Accordingly, ϕ_i^{sat}, $\hat{\phi}_i$ and $\mathscr{P}$ are assumed unity in the calculation of the liquid vapor concentrations in equilibrium with the surrounding air. Insolubility of air in the liquid mixture was also assumed. The phase envelope of the *n*-heptane–methanol mixture is also calculated because it gives some insight in the non-ideal liquid behavior. In this case, real gas behavior is used and $\mathscr{V}_i^{\mathrm{L}}$ is again assumed to be the saturated liquid molar volume.

Variable liquid and gas phase properties have been used in the computations. The liquid mixture molar volume, specific heat and latent heat are evaluated by assuming that the partial molar property is identical to the pure liquid property (ideal solution). The thermal conductivity is calculated through Filippov equation [17] and the mass diffusion coefficient is calculated using Vignes' equation [17], using Wilson's equation to determine the variation of the activity coefficient with composition. The pure liquid diffusion coefficients are predicted by the Tyn and Calus

method [17]. The liquid methanol specific heat is calculated by the Rowlinson–Bondi equation [17] based on known data [20]. The pure liquid densities are assumed to be identical to the saturated density and determined by the modified Rackett equation [17], based on experimental data [18]. The gas mixture density and specific heat are determined by assuming ideal gas behavior. The gas viscosity is determined by Wilke's method [17] and the gas thermal conductivity is calculated by the Wassiljewa equation with the Mason–Saxena modification [17]. The gas-phase diffusion coefficients are approximated to be the coefficients for diffusion of the pure component in air, for which correlations are given by Vargaftik [18]. The pure gas specific heat is approximated by the ideal-gas specific heat for *n*-heptane and by a correlation coupled with the ideal-gas behavior for methanol. The pure component gas thermal conductivities are determined by correlations based on experimental data and the Roy–Thodos method [17] for temperature ranges where data are not available. All the remaining liquid and gas properties are obtained from correlations based on experimental data from Vargaftik [18] and Gallant [20], with small mean errors (around 1–5%).

THE CONTROL-VOLUME METHOD OF LINES

The method of lines uses finite-difference approximations of derivatives to transform a parabolic partial differential equation to a system of ordinary differential equations [21]. Instead of the conventional finite-difference discretization, the control-volume method [22] should be used because it satisfies the global balances even for coarse grids. This combined methodology has been successfully applied to turbulent pipe flow [23]. The difficult task in this method is the solution of the resulting system of ordinary differential equations, which could be quite stiff. However, quite powerful solvers for differential and algebraic–differential systems have been developed [24, 25], which are able to handle the very stiff problems originating from the application of the method of lines.

Using the dimensionless variables defined in the nomenclature and the control-volume discretization technique, equations (2)–(7) can be reduced to a nonlinear system of ordinary differential equations for β, Y_{1_i} and Θ_i, $i = 0, \ldots, n$, where i represents the control-volume centers. The numerical integration was carried out using DAWRS (Differential–Algebraic Waveform Relaxation Solver) ([25, 26]). The system Jacobian is numerically calculated and the absolute and relative tolerances are set to 10^{-6}, which are guaranteed by the DAWRS algorithm. Computations can be performed for any number of grid points. The computational mesh is obtained by an exponential transformation of a uniform mesh in order to increase its density near the surface, where the largest gradients occur. Further details of the solution can be found in ref. [27].

RESULTS AND DISCUSSION

A heptane–methanol mixture, for which an almost complete set of data is available from different sources [16–18, 20, 28], was chosen. Moreover, this mixture is highly non-ideal and it resembles the methanol–gasoline mixture, due to its similar physical properties. Although quite desirable, the calculations for the non-ideal liquid mixtures used by Wang and Law [3] were not performed due to lack of data on thermophysical properties and phase equilibrium. In the following, computational results will be shown for the vaporization of droplets with an initial radius of 50 μm and initial temperature of 300 K, in a stagnant environment at 1500 K and 10 atm. The reference temperature, T_r, is 400 K and the reference properties are the initial properties of the pure liquid or mixture.

Figures 1(a) and (b) show the convergence of this

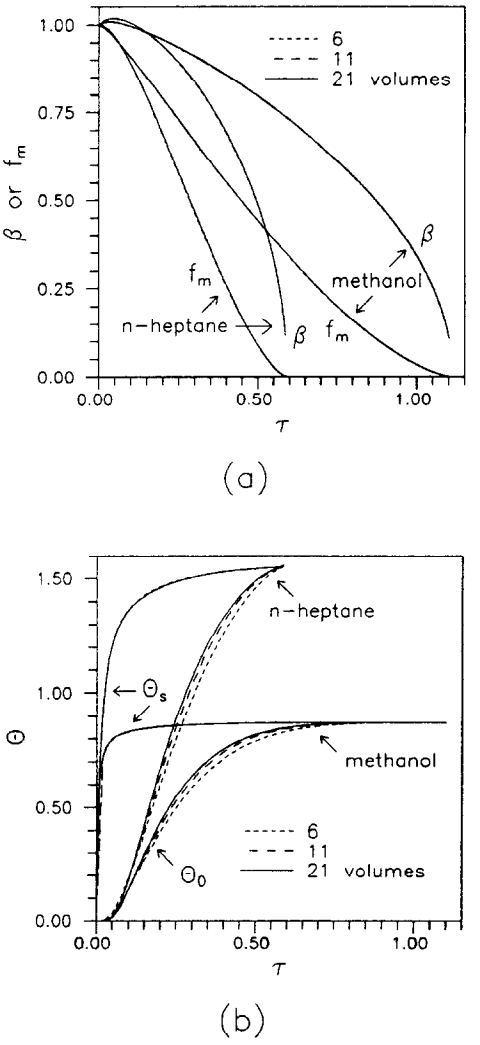

FIG. 1. Vaporization of monocomponent droplets calculated with the complete diffusive model—convergence of the control-volume method of lines. (a) Dimensionless radius and droplet mass, (b) dimensionless center and surface temperature.

method for the vaporization of pure methanol and pure *n*-heptane for 6, 11 and 21 control volumes. Figure 1(a) shows the time variation of the dimensionless radius and the fraction of the droplet mass. The results are practically coincident for the three computations with different number of control volumes. Figure 1(b) shows the transient behavior of the center and surface dimensionless temperature. The computations for the surface temperature are coincident and those for the center temperature agree very well. It should be noticed that the definition of τ varies for each substance, because it is based on the initial α. Figures 2(a) and (b) show the results for the vaporization calculation of a mixture of *n*-heptane–methanol with equal initial mass fractions. Again, excellent convergence is achieved for β and f_m and very good convergence is achieved for the dimensionless center temperature. The dimensionless surface temperature has a complex behavior but very good convergence is achieved as well. Similar convergence behavior is obtained for the transient behavior of all droplet characteristics in all cases, and good convergence is also achieved in the representation of the internal fields (temperature, concentration, velocity and properties).

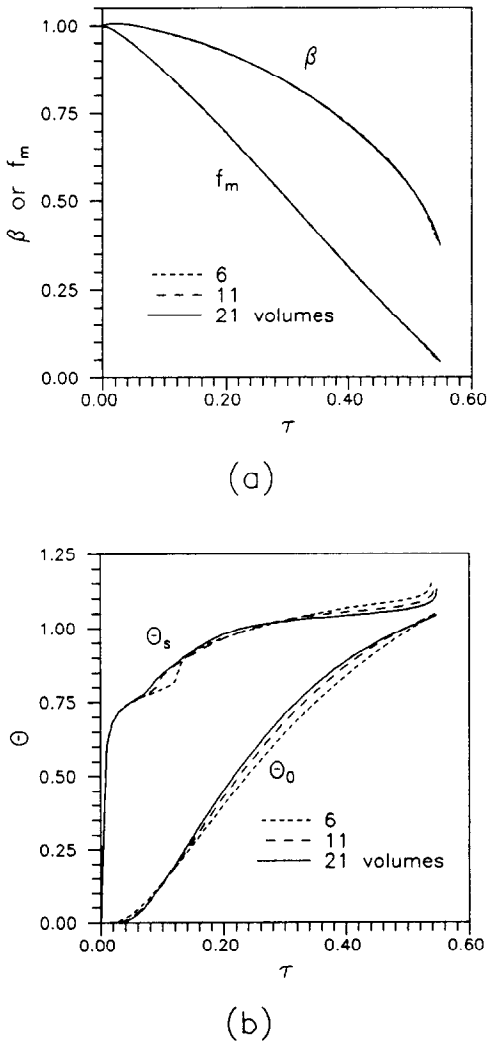

FIG. 2. Vaporization of an *n*-heptane–methanol droplet calculated with the complete diffusive model—convergence of the control-volume method of lines. (a) Dimensionless radius and droplet mass, (b) dimensionless center and surface temperature.

Mono-component droplet: effect of density variation

Since the numerical scheme has proved to be effective, the effect of droplet dilation on its vaporization can now be evaluated. To do so, a second simulation for each pure component case was performed for exactly the same conditions, but the density was considered constant and equal to its initial value. Figures 3(a)–(d) compare the previous results with those obtained with the constant density assumption. Figure 3(a) shows β and f_m for both methanol and *n*-heptane droplets. It can be seen that the allowance for variable density decreases the droplet lifetime up to 15–20%. The transient behavior of the dimensionless temperature and mass vaporization rate are shown in Figs. 3(b) and (c), respectively. It is interesting to note that the variable-density cases present larger vaporization rates during the transient surface heating. The consequence of this is clearly seen in Fig. 3(d), which shows the total rate of energy transfer from the gas to the liquid phase along the droplet lifetime. The integral of this curve gives the total energy necessary to evaporate the droplet. As can be seen from Fig. 3(d), the variable-density case needs less energy to vaporize the same droplet under the same conditions, because a larger fraction of the total droplet mass is vaporized under lower temperatures during the droplet heating (see f_m in Fig. 3(a) and Θ_s in Fig. 3(c)). Of course, the generated vapor is at a lower temperature. The energy necessary for droplet vaporization decreases from 0.267 to 0.197 mJ, for the heptane droplet, and from 0.542 to 0.460 mJ, for the methanol droplet. These figures correspond to 26 and 15% reductions, respectively. The reduction is larger for *n*-heptane because transient surface heating is present over the entire droplet lifetime.

The increase in the rate of heat transfer is caused by the convection induced by the droplet dilation (see equation (7)). The dimensionless radial velocity profiles for several times are shown in Fig. 4 for the *n*-heptane droplet. Initially zero, the velocity at each radial position increases to a maximum and then decreases, reaching zero when the droplet heating finishes. It should be noted that $\partial V/\partial\eta$ is not zero at the droplet center. From equation (1) and assuming that $\rho = \rho(T, Y_1)$ for a bicomponent droplet, it can be shown that

$$\frac{\partial v}{\partial r} = \frac{-1}{3\rho}\left(\frac{\partial \rho}{\partial T}\frac{\partial T}{\partial t} + \frac{\partial \rho}{\partial Y_1}\frac{\partial Y_1}{\partial t}\right) \quad \text{at } r = 0 \qquad (13)$$

which is different from zero as long as there is any

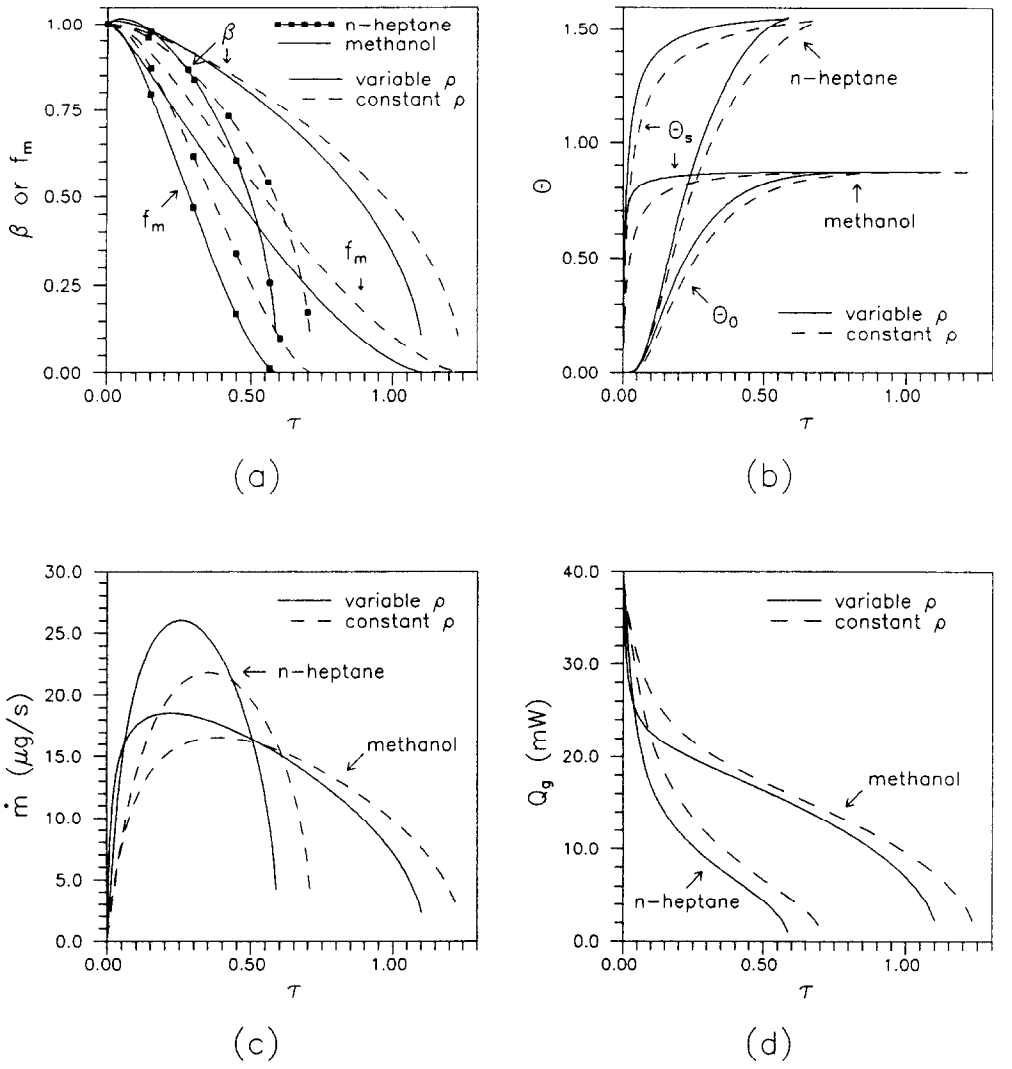

FIG. 3. Vaporization of monocomponent droplets—influence of density variations. (a) Dimensionless radius and droplet mass, (b) dimensionless center and surface temperature, (c) vaporization rate, (d) heat transfer rate.

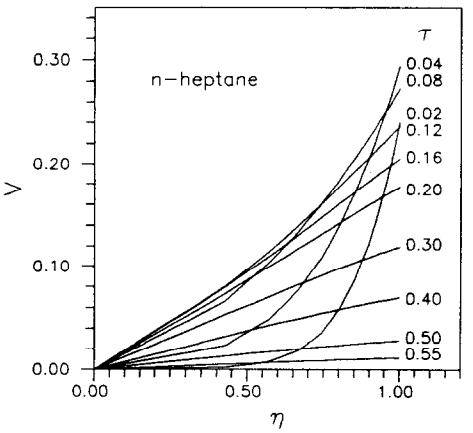

FIG. 4. Vaporization of an *n*-heptane droplet—radial profiles of the velocity induced by density variations.

temporal change of temperature or concentration at the droplet center.

Binary droplet

The phase equilibrium diagram of the *n*-heptane–methanol mixture at 10 atm, calculated with the procedure outlined above, is shown in Fig. 5. This mixture shows an azeotropic point at a heptane molar fraction of about 0.26. For heptane concentrations larger than this value, *n*-heptane tends to be vaporized preferentially, while methanol vaporization is favored for lower concentrations. In the following, results are presented for an *n*-heptane–methanol mixture under the conditions described at the beginning of the Results and Discussion section. Unless stated otherwise, the initial mass fraction is 0.5.

In order to verify the importance of several

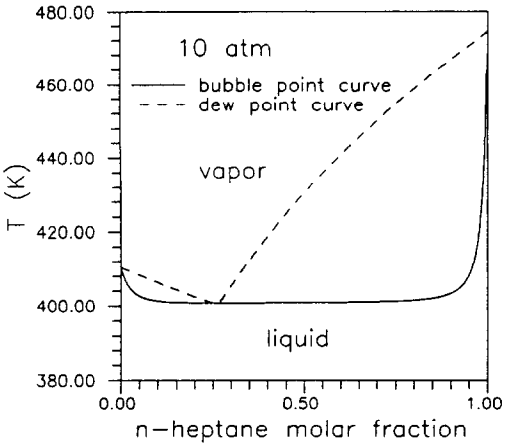

FIG. 5. Phase-equilibrium diagram of the *n*-heptane–methanol mixture at 10 atm.

improvements made to the conventional liquid diffusion model, simulations have been performed where each one of the improvements is disabled. Afterwards, the conventional liquid-phase diffusion model is retrieved by disabling all the improvements. Thus, Figs. 6(a)–(e) compare the vaporization results obtained for several particular cases to those of the complete diffusive model developed in this work. The considered particular cases retrieved from the complete model are: (a) constant density (equal to initial density), (b) ideal phase equilibrium at the droplet surface ($a_i = 1$), (c) no interdiffusion terms in the energy equation and its boundary condition and (d) the conventional diffusive model (obtained by considering all of the above assumptions). Figure 6(a) shows the time variation of the dimensionless droplet radius and the fractional droplet mass. The differences in the droplet lifetimes obtained through the several models is quite remarkable. The conventional diffusive model predicts a lifetime 60% higher than that predicted by the complete model. Figure 6(a) highlights the importance of each improvement to the model in predicting the droplet lifetime. The major contribution to the lifetime variation is the allowance for variable density, but the influence of the interdiffusion term in the predicted vaporization is quite appreciable. As in the pure-substance case, temperature and concentration changes cause a non-uniform droplet dilation, which induces a radial convection. The induced radial velocity field is similar to that of the pure *n*-heptane case presented above. This induced convection and the interdiffusion are responsible for the increase in the rate of heat and mass transfer, which enhances vaporization. The dimensionless temperature profiles are shown in Fig. 6(b). When non-ideal phase equilibrium is used, the surface temperature shows a peculiar behavior, with an abrupt change of curvature, which disappears when the ideal equilibrium is assumed. The non-ideality of the phase equilibrium is what mainly modifies the behavior of the surface temperature, especially the maximum achieved surface temperature. The influence of variable density is also appreciable. All the results except those obtained with the conventional diffusive model show a sharp increase in the surface temperature near the end of the droplet lifetime. This and other peculiar behaviors near the end of droplet vaporization will be examined below. Figure 6(c) shows the temporal variation of the droplet-surface and droplet-center *n*-heptane mass fraction. Allowing for variable density modifies the time necessary to reach the quasi-steady state, while the assumption of phase equilibrium at the surface is responsible for the maximum value of mass fraction achieved. Figure 6(d) shows the mass vaporization rates. The processes included in the complete diffusive model lead to an increase in the instantaneous rate of vaporization. Figure 6(e) shows the total rate of heat transfer from the gas phase into the liquid phase. As in the case of pure substances, each improvement made to the conventional diffusive model leads to a decrease in the total energy necessary to vaporize the droplet. The total energy requirement for droplet vaporization is predicted to be 0.425 mJ by the conventional diffusive model and 0.223 mJ, almost a 50% reduction, by the model developed in this work. If density changes are not taken into account, a large error is introduced in the prediction of $\dot{m}$ and Q_G. Since liquid vaporization is the controlling factor in heavy fuel combustion, these reductions in energy requirement and droplet lifetime should have a large impact in full combustor simulations.

Since phase equilibrium has been shown to control the surface behavior, Fig. 6(f) shows the gas-phase mass fractions of *n*-heptane and methanol, the fractional vaporization rate of *n*-heptane and the surface liquid mass fraction of *n*-heptane for the calculations using the model developed in this work, with non-ideal and ideal phase equilibrium. In both cases, after a short transient state, a quasi-steady state is achieved which continues until near the end of the droplet lifetime. The behavior of the fractional vaporization rate and the liquid surface mass fraction is greatly influenced by the type of phase equilibrium used. As shown by the above results, the surface equilibrium temperature and concentrations for non-ideal phase equilibrium are quite different from those obtained with the ideal equilibrium assumption, even though the time variation of the droplet radius is well predicted. Thus, studies of micro-explosion phenomena of non-ideal liquid mixtures must include the non-ideal phase equilibrium as well as the non-ideal behavior of superheating temperature. Moreover, the higher heat and mass transfer rates predicted by the complete model may explain the difference between experimental data and predictions of the radial position of bubble formation in droplet micro-explosion [8].

As mentioned earlier, the results obtained with the complete model show an increase in the surface temperature, *n*-heptane fractional mass vaporization rate, the total vaporization rate, and a small decrease in the

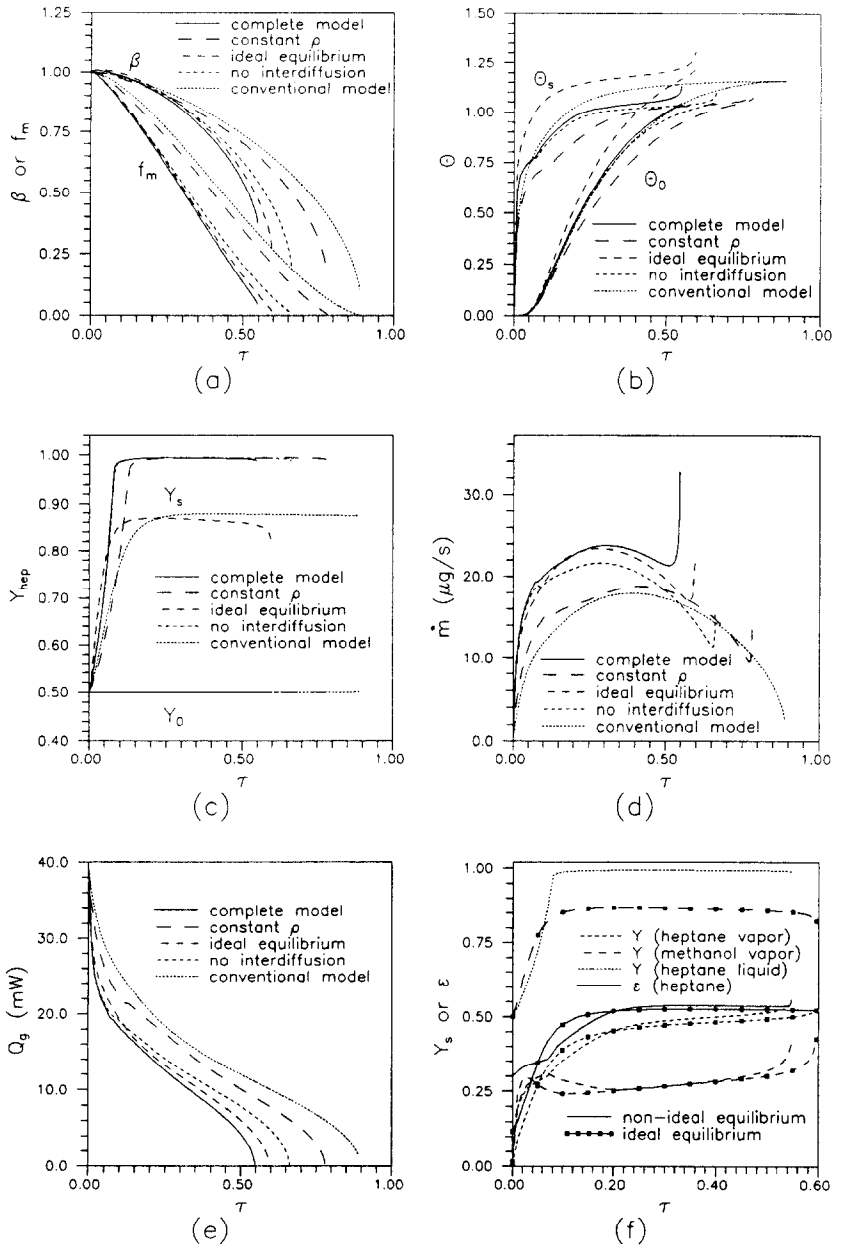

FIG. 6. Vaporization of an *n*-heptane–methanol droplet calculated with the complete diffusive model—evaluation of the improvements made to the conventional model. (a) Dimensionless radius and droplet mass, (b) dimensionless center and surface temperature, (c) surface and center *n*-heptane mass fraction, (d) vaporization rate, (e) heat transfer rate, (f) methanol and *n*-heptane mass fraction and *n*-heptane vaporization rate.

n-heptane surface mass fraction towards the end of the droplet lifetime. Moreover, the sum of fuel vapor mass fractions at the droplet surface tends to unity. This is a strong indication of the occurrence of flash vaporization. The physical reasoning is the following: when the mass diffusion wave reaches the droplet center there is not enough methanol to diffuse towards the droplet surface to maintain the quasi-steady vaporization state. Then less methanol is vaporized and thus the *n*-heptane fractional mass vaporization rate increases while its surface concentration decreases. Since the latent heat of methanol is larger than that of *n*-heptane, more energy is available at the droplet surface for liquid heating, and the surface temperature thus increases. As the surface temperature increases and the *n*-heptane concentration decreases, the mixture at the surface approaches its bubble point. Under these conditions, the spherical

shell near the surface vaporizes very rapidly. However, the inner shells have lower concentrations of *n*-heptane and are at almost the same temperature. Thus, the new surface conditions tend to surpass the mixture bubble point and the process of rapid vaporization continues until the whole droplet undergoes flash vaporization.

In order to confirm the model's ability to predict flash vaporization, other simulations have been performed under the same conditions, but with different initial compositions. The dimensionless radius, the dimensionless surface temperature, the surface mass fraction, and the mass vaporization rate are shown in Figs. 7(a)–(d), respectively. It can be seen that methanol is vaporized preferentially for the cases where $Y^l_{hep}(0) \geqslant 0.35$, and that *n*-heptane vaporization is favored for $Y^l_{hep}(0)$ below this value. In the cases with the three lowest values for $Y^l_{hep}(0)$, Figs. 7(a) and (d) show lower vaporization rates, which result from the lower value of the quasi-steady surface temperature (shown in Fig. 7(b)). This lower surface temperature is caused by the preferential vaporization of *n*-heptane, for $Y^l_{hep}(0) = 0.25$ and 0.30, or by the insufficient concentration of *n*-heptane to establish a large concentration gradient at the surface (see Fig. 7(c)). Accordingly, flash vaporization does not occur in these cases. The simulations with $Y^l_{hep}(0) = 0.45$ and 0.50 show the phenomenon of flash vaporization, as described in the preceding paragraph. The simulation with $Y^l_{hep}(0) = 0.40$ is in a transition region, where there is enough *n*-heptane to promote a large concentration gradient at the surface (Fig. 7(c)), but the resulting equilibrium temperature is not large enough to promote flash vaporization (see Figs. 7(b) and (d)). There is a small temperature increase near the end of the droplet vaporization (Fig. 7(b)), but only after a considerable drop of the surface concentration value, as shown in Fig. 7(c). We have found that flash vaporization occurs for $Y^l_{hep}(0) > 0.50$ as well. Thus, the necessary conditions for the occurrence

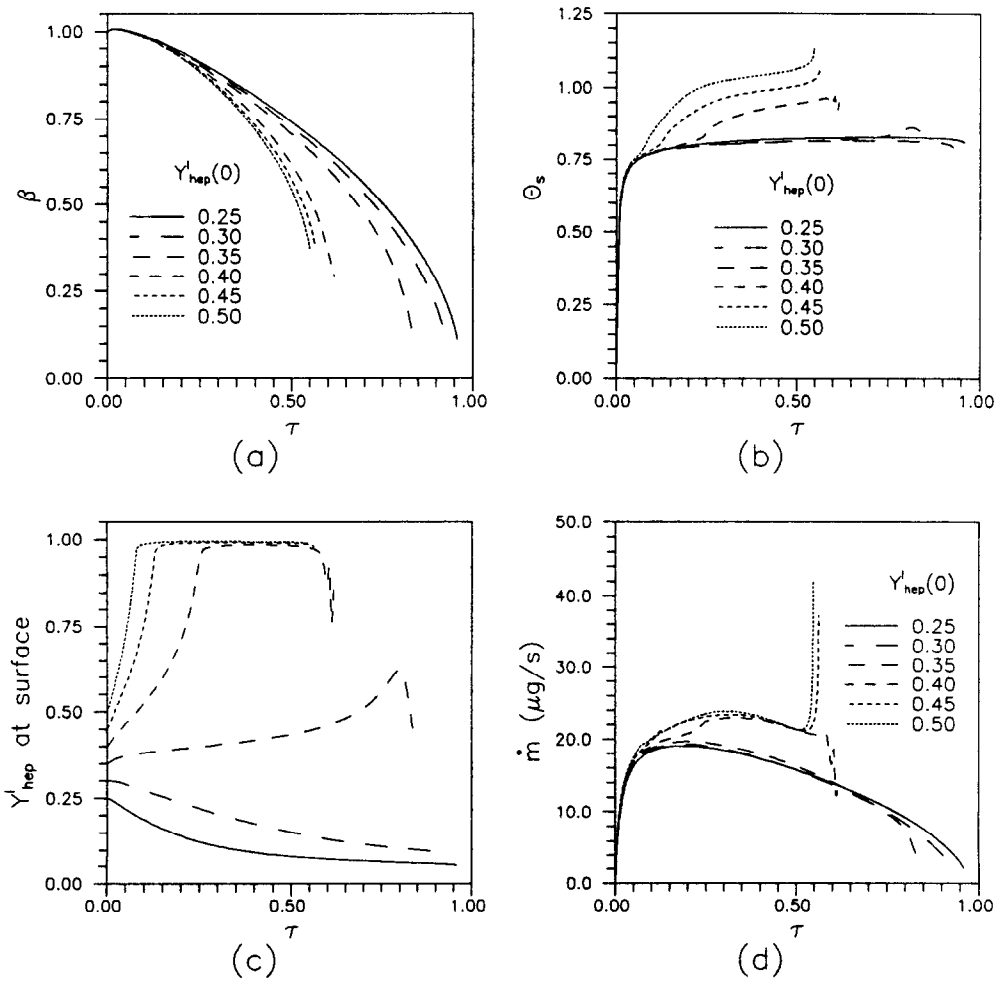

FIG. 7. Vaporization of an *n*-heptane–methanol droplet calculated with the complete diffusive model for several initial compositions. (a) Dimensionless radius, (b) dimensionless surface temperature, (c) surface *n*-heptane mass fraction, (d) vaporization rate.

of flash vaporization can be drawn from the above results. First, the component which vaporizes preferentially must have the largest latent heat. Second, there must be enough of the other component to establish a large concentration gradient at the surface, which must also lead to a quasi-steady temperature close enough to the mixture bubble point. For the cases analyzed, those with $Y^l_{hep}(0) \geqslant 0.35$ satisfy the first condition, but only those with $Y^l_{hep}(0) \geqslant 0.45$ also satisfy the second condition. Moreover, the inability of the conventional diffusive model to predict flash vaporization in the case shown in Figs. 6(a)–(e) is due to the assumptions implicit in that model. Namely, the ideal-equilibrium hypothesis leads to a lower concentration gradient at the surface, which, with the lower heat transfer transport caused by the neglect of dilation and interdiffusion, results in a lower quasi-steady surface temperature. Thus, the second condition stated above is violated, and no flash vaporization is predicted.

To the best of our knowledge, it is the first time that a vaporization model is able to predict the fast droplet vaporization at the end of the lifetime of a multicomponent droplet. It is believed that the experimentally observed weak sparkle at the end a monocomponent or multicomponent droplet combustion process is due to the flash vaporization (soot caused by high local fuel vapor concentration would be responsible for the flame luminosity). In the case of a monocomponent droplet, impurities should be present to cause flash vaporization.

Although the above results have been obtained for stagnant environments (or no relative droplet–gas velocity), the dynamics of induced convection caused by dilation can be introduced to existing convective–diffusive models [6, 7]. For instance, in the limit of very fast internal circulation, there is heat diffusion normal to the internal streamlines and thus there would be a velocity field normal to these streamlines caused by non-uniform dilation. Therefore, an enhancement in the heat and mass transfer rates is also expected for vaporization in convective environments.

CONCLUSIONS

A modified diffusive liquid vaporization model for multicomponent droplets has been developed which includes spatially and time variable density, the interdiffusion terms in the energy equation and in its boundary condition, variable thermophysical properties and non-ideal phase equilibrium. This complete diffusive model is used to simulate the vaporization of droplets of *n*-heptane, methanol, and their mixture. The importance of each improvement to the conventional model is quantified. From the analysis, the following conclusions can be drawn:

- The neglect of the interdiffusion terms leads to small errors in maximum surface droplet temperature and concentration but a considerable droplet lifetime error is generated.
- The variation of density with temperature and concentration leads to a radial velocity field which greatly enhances the heat and mass transfer rates. This induced convection, together with the interdiffusion of species, decreases the droplet lifetime (up to 40%) and energy requirement for droplet vaporization (up to 50%) in comparison to the conventional model predictions. This induced convection mechanism is also expected to occur for droplets with internal circulation.
- The non-ideal phase equilibrium must be used in the vaporization of non-ideal liquid mixtures. Although the ideal equilibrium assumption leads to a good prediction for the droplet radius history, the surface temperature and concentrations are very poorly evaluated.
- The experimentally observed weak sparkle at the end of the combustion of a fuel droplet can be explained by the complete model applied to a binary (or multicomponent) mixture. The model indicates that the observed phenomenon corresponds to flash vaporization.

The usage of the complete diffusion model in the global simulation of combustors and in studies of droplet micro-explosions should lead to improvements in the agreement between theory and experiments.

Acknowledgements—The first author would like to acknowledge the financial support from CNPq, Grant No. 202129/90.0. This research was supported in part by the University of California, Irvine, through an allocation of computer time. Some computations were performed on the Cray Y-MP at the San Diego Supercomputing Center.

REFERENCES

1. C. K. Law, Recent advances in droplet vaporization and combustion, *Prog. Energy Comb. Sci.* **8,** 169–199 (1982).
2. W. A. Sirignano, Fuel droplet vaporization and spray combustion theory, *Prog. Energy Comb. Sci.* **9,** 291–322 (1983).
3. C. H. Wang and C. K. Law, Microexplosion of fuel droplet under high pressure, *Combust. Flame* **59,** 53–62 (1985).
4. C. K. Law, Unsteady droplet vaporization with droplet heating, *Combust. Flame* **26,** 17–22 (1976).
5. C. K. Law and W. A. Sirignano, Unsteady droplet combustion with droplet heating—II: Conduction limit, *Combust. Flame* **28,** 175–186 (1977).
6. S. Prakash and W. A. Sirignano, Theory of convective droplet vaporization with unsteady heat transfer in the circulating liquid phase, *Int. J. Heat Mass Transfer* **23,** 253–268 (1980).
7. M. Abramzon and W. A. Sirignano, Droplet vaporization model for spray combustion calculations, *Int. J. Heat Mass Transfer* **32,** 1605–1618 (1989).
8. C. H. Wang, X. Q. Liu and C. K. Law, Combustion and microexplosion of freely falling multicomponent droplets, *Combust. Flame* **56,** 175–197 (1984).
9. C. K. Law, Internal boiling and superheating in vaporizing multicomponent droplets, *A.I.Ch.E. Jl* **24,** 626–632 (1978).

10. P. Lara-Urbaneja and W. A. Sirignano, Theory of transient multicomponent droplet vaporization in a convective field, *Eighteenth Symposium (International) on Combustion*, pp. 1365–1374. The Combustion Institute (1981).
11. C. M. Megaridis and W. A. Sirignano, Numerical modeling of a vaporizing multicomponent droplet, *Twenty-Third Symposium (International) on Combustion*, University of Orleans, France. The Combustion Institute (1990).
12. P. L. C. Lage and R. H. Rangel, Single droplet vaporization including thermal radiation absorption, *J. Thermophy. Heat Transfer* **7** (1993).
13. J. C. Lasheras, A. C. Fernandez-Pello and F. L. Dryer, Experimental observations on the disruptive combustion of free droplets of multicomponent fuels, *Combust. Sci. Technol.* **22,** 195–209 (1980).
14. P. L. C. Lage, R. H. Rangel and C. M. Hackenberg, Multicomponent heat and mass transfer for flow over a droplet, *Int. J. Heat Mass Transfer* **36,** 3573–3581 (1993).
15. R. B. Bird, W. E. Steward and E. N. Lightfoot, *Transport Phenomena*, p. 658. Wiley, New York (1960).
16. S. Ohe, *Vapor–liquid Equilibrium Data*. Elsevier, Amsterdam (1989).
17. R. C. Reid, J. M. Prausnitz and B. E. Poling, *The Properties of Gases and Liquids* (4th Edn). McGraw-Hill, New York (1987).
18. N. B. Vargaftik, *Tables on the Thermophysical Properties of Liquids and Gases* (2nd Edn). Hemisphere, New York (1975).
19. D.-Y. Peng and D. B. Robinson, A new two-constant equation of state, *Ind. Engng Chem., Fundam.* **15,** 59–64 (1976).
20. R. W. Gallant, *Physical Properties of Hydrocarbons*, Vol. 1. Gulf, Houston, Texas (1968).
21. D. Zwillinger, *Handbook of Differential Equations*. Academic Press, New York (1989).
22. S. V. Patankar, *Numerical Heat Transfer and Fluid Flow*. McGraw-Hill, New York (1980).
23. J. C. Morales, A. Campo and U. Lacoa, Analysis of turbulent convective heat transfer in circular pipes by the method of lines and control volumes (molcv), *Physico-Chemical Hydrodynamics* **10,** 65–76 (1988).
24. K. E. Brenan, S. L. Campbell and L. R. Petzold, *Numerical Solution of Initial-Value Problems in Differential-Algebraic Equations*. North-Holland, New York (1989).
25. A. R. Secchi, M. Morari and E. C. Biscaia, Jr., DAWRS: A differential-algebraic system solver by the waveform relaxation method, *Sixth Distributed Memory Computing Conference (DMCC6)*, Portland, Oregon (1991).
26. A. R. Secchi, M. Morari and E. C. Biscaia, Jr., The waveform relaxation method for concurrent dynamic process simulation, *A.I.Ch.E. Meeting*, Los Angeles, California (1991).
27. P. L. C. Lage, Multicomponent droplet vaporization in convective and radiative fields (in Portuguese), D.Sc. Thesis, COPPE/UFRJ, Rio de Janeiro, Brazil (1992).
28. G. A. Melhem, R. Saini and B. M. Goodwin, A modified Peng–Robinson equation of state, *Fluid Phase Equil.* **47,** 189–237 (1989).